

Indexing current-voltage characteristics using a hash function

T. Tanamoto,¹ S. Furukawa,¹ R. Kitahara,¹ T. Mizutani,² K. Ono,³ and T. Hiramoto²

¹*Department of information and science, Teikyo University, 1-1 Toyosatodai, Utsunomiya, Tochigi 320-8551, Japan^{a)}*

²*Institute of Industrial Science and the VLSI Design and Education Center, University of Tokyo, Tokyo, Japan*

³*Advanced Device Laboratory, RIKEN, Wako-shi, Saitama 351-0198, Japan*

(Dated: 21 February 2025)

Differentiating between devices of the same size is essential for ensuring their reliability. However, identifying subtle differences can be challenging, particularly when the devices share similar characteristics, such as transistors on a wafer. To address this issue, we propose an indexing method for current-voltage characteristics that assigns proximity numbers to similar devices. Specifically, we demonstrate the application of the locality-sensitive hashing (LSH) algorithm to Coulomb blockade phenomena observed in PMOSFETs and nanowire transistors. In this approach, lengthy data on current characteristics are replaced with hashed IDs, facilitating identification of individual devices, and streamlining the management of a large number of devices.

As transistor sizes continue to shrink, the number of transistors that factory engineers must analyze increases significantly¹. Classifying devices within a wafer is essential, as their characteristics can vary depending on their location, such as whether they are positioned at the edge or center of the wafer²⁻⁴. As data volume grows, managing this vast amount of information becomes increasingly complex. While automated measurements combined with statistical data analysis are now standard practices⁵⁻⁷, the detailed analysis of individual devices still heavily depends on the expertise of experimenters and engineers.

A Physically Unclonable Function (PUF) is an important hardware security mechanism that protects personal information by providing a unique ID for each device at a low cost⁸⁻¹³. Smaller devices are more susceptible to defects and traps, leading to greater variability among them. Controlling atomic order is either impractical or prohibitively expensive¹⁴. In Ref. ¹⁵, we proposed a PUF that utilizes the effects of trap sites, which can be observed in the subthreshold region as a fingerprint of transistors. Distinguishing devices using image recognition algorithms has the advantage of enabling the direct application of a wide range of recognition techniques, including artificial intelligence. In Ref. ¹⁵, we employed *OpenCV* algorithms¹⁶⁻¹⁹ to differentiate between chips based on variations in the Coulomb diamond images. However, this method requires storing image data, which generally demands a large amount of memory. Therefore, developing a more efficient method for distinguishing devices is crucial for applying PUF to nanodevices.

To efficiently manage a large number of devices including the PUF application, assigning each device a unique identifier based on its characteristics would be beneficial. A direct approach is to apply clustering techniques to the current-voltage (*I-V*) characteristics, enabling the visualization of differences in device performance²⁰. However, conventional clustering may not always effectively distinguish subtle differences between devices (see appendix). Instead of analyzing all *I-V*

characteristics individually, assigning an ID that encapsulates the current characteristics of each device would simplify management and reduce the engineers' workload.

Locality-Sensitive Hashing (LSH) is a method designed for searching data in high-dimensional spaces by increasing the likelihood that similar data points share the same hash value²¹⁻²⁵. Indyk and Motwani introduced this technique to mitigate the "curse of dimensionality"²¹. The effectiveness of LSH has been demonstrated in various applications, including image search²⁶, document similarity search, genetic data analysis²⁷, music recommendation systems²⁸, and anomaly detection in sensor data²⁹. For example, image search engines utilize LSH to rapidly identify images similar to those uploaded by users within extensive databases. LSH filters have been proposed for video anomaly detection²⁶ and have also been applied to detect anomalies in sensor data collected from IoT devices²⁹.

In this study, we apply LSH to device datasets and investigate the appropriate hash function parameters that best fit the experimental data. We evaluate two distinct types of devices: PMOSFETs operating within the Coulomb blockade regions and nanowire transistors. Coulomb blockade is a significant phenomenon observed in nanodevices, and the Coulomb diamond patterns reveal clear differences between devices, allowing for precise identification and classification. By contrast, nanowire transistors exhibit monotonous *I-V* characteristics, making differentiation more challenging. We demonstrate that LSH effectively distinguishes these devices. The characteristics of devices can shift owing to various factors, and measurements taken on different days may yield different results for the same device. This variability is particularly relevant for PUF applications. We compare the hash IDs derived from the *I-V* characteristics, highlighting the robustness and reliability of our approach.

Hash function— In LSH, a given data is converted by the hash function defined by²¹

$$h_{a,b}(\mathbf{v}) = \left\lfloor \frac{\mathbf{a} \cdot \mathbf{v} - bw}{w} \right\rfloor \quad (1)$$

where \mathbf{v} represents the given dataset, which in our case consists of the experimentally obtained I_D values. The pa-

^{a)}Electronic mail: tanamoto@ics.teikyo-u.ac.jp

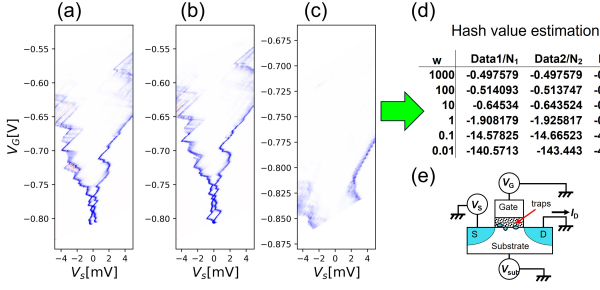


FIG. 1. (a)(b)(c) Coulomb diamonds were observed in the differential conductance characteristics (dI_D/dV_S) of trap states in a conventional pMOSFET with a channel length $L = 125$ nm and width $W = 220$ nm at a temperature of $T = 1.54$ K. A silicon oxynitride layer was used for the gate dielectric. Although these devices share the same layout parameters (length and width), they exhibit different characteristics owing to variations in the distribution of trap sites. Additionally, the hash values for datasets (a), (b), and (c) are provided in section (d). N_i represents the number of data points for each dataset.

parameters \mathbf{a} and \mathbf{b} are a randomly generated vector and a random number within the range $\{0, 1\}$, respectively. The segment size, w , determines how the given data is partitioned. Additionally, multiple sets of \mathbf{a} and \mathbf{b} are prepared, which are called "bucket", and are given by $g(\mathbf{v}) = \{h_{\mathbf{a}_1, \mathbf{b}_1}(\mathbf{v}), h_{\mathbf{a}_2, \mathbf{b}_2}(\mathbf{v}), \dots, h_{\mathbf{a}_{n_{\text{buk}}}, \mathbf{b}_{n_{\text{buk}}}}(\mathbf{v})\}$, where n_{buk} is the number of elements in the bucket. Conventionally, many sets of the buckets are prepared, such as $\{g_0(\mathbf{v}), g_1(\mathbf{v}), \dots\}$; however, here we only consider one $g(\mathbf{v})$ to observe what kinds of parameters are appropriate for distinguishing the devices.

Conventional datasets, such as images, are typically represented using binary values 0, 1, and the distance between data points is computed based on these binary representations. By contrast, I - V characteristics are expressed as real numbers, often in exponential notation. Although one approach is to discretize these real numbers into digital values, this introduces additional computational overhead and potential loss of precision. Therefore, it is preferable to process the raw experimental data directly to maintain accuracy and minimize unnecessary transformations.

In Eq. (1), w represents the width of the bucket, which plays a crucial role in distinguishing similar data points while ensuring that distinct data points are assigned to separate buckets. Selecting an appropriate value for w is essential for effectively differentiating between device data. In the following section, we will determine suitable values for w by first estimating the direct Euclidean distance among the data. Our analysis will ultimately show that the optimal choice for w is the standard deviation of the raw data.

One of the key advantages of using LSH is its ability to significantly reduce the number of data points that require processing. Given N devices and defining n_d as the number of elements in the I - V dataset, conventional processing would involve handling Nn_d data points. However, by assigning hash IDs to each I - V characteristic, the computational burden is drastically reduced to just N numerical values, making the approach highly efficient for large-scale applications.

Results— We show the result of the application of LSH to Coulomb blockade and nanowire transistors, and the appropriate choice of the hash parameter w is estimated.

Coulomb blockade— Figure 1 illustrates the Coulomb diamond structure that arises owing to trap sites at the Si/SiO₂ interface in a 130 nm PMOSFET^{15,30,31}. Figures 1(a) and 1(b) display Coulomb diamonds measured from the same device on different days, while Figure 1(c) presents data from a different device. Despite having identical gate lengths and widths and being fabricated on the same wafer, the devices exhibit distinct Coulomb diamond characteristics due to variations in trap profiles. These uncontrollable trap distributions provide a unique fingerprint, making them well-suited for PUF applications. Additionally, the discrepancy between Figures 1(a) and 1(b) is attributed to changes in the measurement environment, such as variations in the applied force from the needle of the apparatus or fluctuations in temperature.

First, we estimate the Euclidean distance between the datasets, where the Euclidean distance between the two data points, A and B , is defined by the equation:

$$d_{A,B} = \sqrt{\sum_{j=1}^{n_d} \left(\frac{dI_{D,j}^A}{dV_G} - \frac{dI_{D,j}^B}{dV_G} \right)^2}. \quad (2)$$

The dataset shown in Fig. 1 is represented as $(V_G, V_D, \frac{dI_D}{dV_G})$. To facilitate analysis, this data is converted into a two-dimensional representation with coordinates (x, y) , where y corresponds to $\frac{dI_D}{dV_G}$. Then, the pair (V_G, V_D) is treated as a single axis given by $x = (V_G, V_D)$. The number n_d refers to the total data points, calculated as the product of the number of V_G values and the number of V_D values. To ensure a fair comparison between the two datasets, we must use a consistent x -axis. However, the current data for $x = (V_G, V_D)$ shown in Figs. 1(a) to 1(c) do not align. To address this issue, we identify and select a common (V_G, V_D) region that overlaps across the three datasets.

The Euclidean distances between the data points are calculated by $d_{(a),(b)} = 1012.78$, $d_{(b),(c)} = 1061.95$, and $d_{(a),(c)} = 1297.23$. The difference in the Euclidean distance between the same devices ((a) and (b)) is approximately 4.74%, whereas the difference between the different devices ((a) and (c)) is approximately 25.1%. This demonstrates that the Euclidean distances serve as a metric to distinguish between devices. However, as the number of devices N increases, the Euclidean distances $\sqrt{N(N-1)}$ must be managed, which is inefficient. Therefore, indexing devices is crucial.

To address this issue, we apply Eq.(1) to the three datasets shown in Fig. 1. The hash function in Eq.(1) includes a parameter w that needs to be determined. Figure 1(d) presents the hash values for the three Coulomb diamonds using various choices of w . The results indicate that smaller values of w are more effective in differentiating between the devices. Notably, a Euclidean distance of approximately 1000 is insufficient to distinguish between datasets (a) and (c), necessitating an alternative approach. The standard deviations of the original data are estimated as follows: $std_{(a)} = 8.463$, $std_{(b)} = 3.087$, and $std_{(c)} = 8.916$. This suggests that selecting w based on

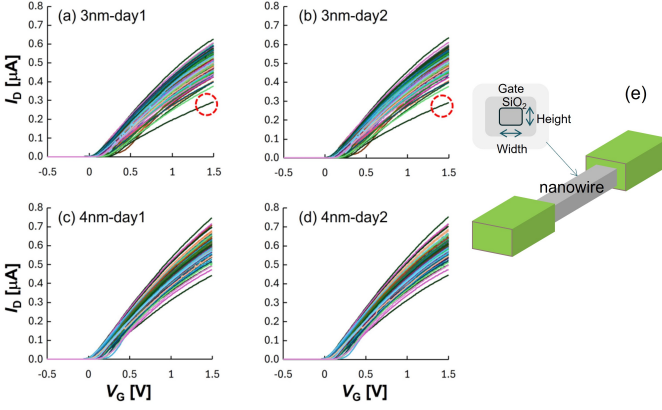


FIG. 2. I_D - V_G characteristics of the GAA silicon nanowire transistor at $V_D = 50$ mV. (a)(b) 3 nm width, and (c)(d) 4 nm width. No.141 (marked by a red circle) in both (a)(b) deviate from others. (e) Schematic of GAA silicon nanowire FET, where $L=100$ nm, $H=3$ nm.

the standard deviation, rather than the absolute Euclidean distance, is more appropriate. From these observations, we conclude that: (1). The same device produced similar hash values. (2). Different devices yield distinct hash values when w is in the order of the standard deviation.

Nanowire transistors— The nanowire transistors do not exhibit specific characteristics, such as Coulomb diamonds. Gate-all-around (GAA) silicon nanowire nFETs with (110)-oriented channels were fabricated on (001) SOI substrates. The height of the nanowire channel (H) is 3 nm, and the channel length (L) is 100 nm³². The detailed fabrication process is described in Refs.^{33–35}. We compared 160 nanowire transistors with widths of 3 and 4 nm, utilizing measurements taken on different days. The I_D - V_G characteristics of the nanowire transistors are presented in Fig. 2. Compared to Fig. 1, all the nanowire data appear similar. As shown in Fig. 2, the I_D - V_G curve of transistor No. 141 (marked by a red circle) is smaller than those of the other transistors. Here, the device number corresponds to the position of the device in the wafer.

First, we estimate the Euclidean distance of the I_D - V_G data as n_d -dimensional data ($n_d = 160$). Figure 3 (a) shows the Euclidean distance between two sets of data observed on different days. The same chip measured on different days (day1 and day2) exhibits small distances, whereas the distances between different sizes (3 and 4 nm) are considerably larger. The average Euclidean distances between the data are as follows: $d_{3nm_{day1}, 3nm_{day2}} = 2.983 \times 10^{-8}$ A, $d_{4nm_{day1}, 4nm_{day2}} = 3.436 \times 10^{-8}$ A, $d_{3nm_{day1}, 4nm_{day1}} = 7.811 \times 10^{-7}$ A, $d_{3nm_{day2}, 4nm_{day2}} = 7.879 \times 10^{-7}$ A. Thus, the Euclidean distance effectively distinguishes devices of different sizes. However, as previously mentioned, managing individual I - V data becomes increasingly cumbersome as the number of devices grows.

To address this issue, we apply indexing using the hash function. Figure 3(b) illustrates the distances between two sets of hash values collected on different days. We have examined the hash values by varying the random numbers $\{a, b\}$.

"[0]" and "[10]" display the results of the first and 11th random number sets. The parameter $w = 10^{-9}$ is selected as the standard deviation of the data, where a detailed analysis of w will be conducted later. It can be observed that the distances between devices of different sizes are significantly larger than those between the same devices measured on different days. This indicates that, instead of relying on the direct data presented in Fig. 3(a), the hash values effectively represent the current-voltage characteristics, providing a more efficient approach to distinguishing between devices.

Here, we analyze the suitable range for the hash values. Figure 4(a) shows the distribution of hash values for four devices, generated using different sets of random numbers, a and b (where $N_{buk} = 10$). It is evident that the hash values shift consistently in the same direction. This observation suggests that while changing the set of random numbers $\{a, b\}$ affects the absolute hash values, the relative hash distances between data points remain unchanged. Focusing on the hash value for chip number 141 (highlighted by the red dotted circles in Figs. 2 and 4(a)), we observe that its hash value is smaller compared to the other devices. This distinction allows us to differentiate devices with varying I - V characteristics using their corresponding hash values. Figure 4(b) illustrates the dependence of the distance ratio on the parameter w , which is defined by:

$$\text{ratio}_{distance} \equiv \frac{dh_{3nm_{day1}, 4nm_{day1}} + dh_{3nm_{day2}, 4nm_{day2}}}{dh_{3nm_{day1}, 3nm_{day2}} + dh_{4nm_{day1}, 4nm_{day2}}}, \quad (3)$$

where $dh_{A,B}$ represents the difference between the two hash values of datasets A and B . The "bucket" displays different sets of $\{a, b\}$. In Fig. 4(b), " σ " denotes the average standard deviation, which is calculated to be 4.56×10^{-8} A, and "distance34" indicates the average Euclidean distance between the 3 and 4 nm devices. A larger distance ratio is beneficial for distinguishing between two devices. Therefore, it is preferable to choose w close to the standard deviation, which aligns with the findings presented in Fig. 1.

Figure 4(c) presents the histogram of the hash value distributions, showing that the 3 and 4 nm devices exhibit distinct peak positions, which enables differentiation between the two sets of transistors overall. However, within the hash value range of 1.6×10^9 to 2.2×10^9 , both 3 and 4 nm devices share similar hash values, making it impossible to determine whether a device belongs to the 3 or 4 nm transistor category in this range. This result suggests that relying on a single hash value is insufficient for effectively distinguishing between the two datasets.

In conventional transistors, both I_D - V_D and I_D - V_G characteristics are provided, allowing us to generate more than a single hash value. This enables the measured values to be treated as vectors. Figure 5(a) illustrates the difference in hash values between 3 nm and 4 nm nanowires for various V_G values. Figure 5(b) presents the Euclidean distance between the two vectors, which are defined as $(h_{V_G=1.2V}^{3nm}, h_{V_G=0.8V}^{3nm}, h_{V_G=0.4V}^{3nm}, h_{V_G=0.0V}^{3nm})$ and $(h_{V_G=1.2V}^{4nm}, h_{V_G=0.8V}^{4nm}, h_{V_G=0.4V}^{4nm}, h_{V_G=0.0V}^{4nm})$. Compared to Figure 5(a), the minimum distance between the vectors in

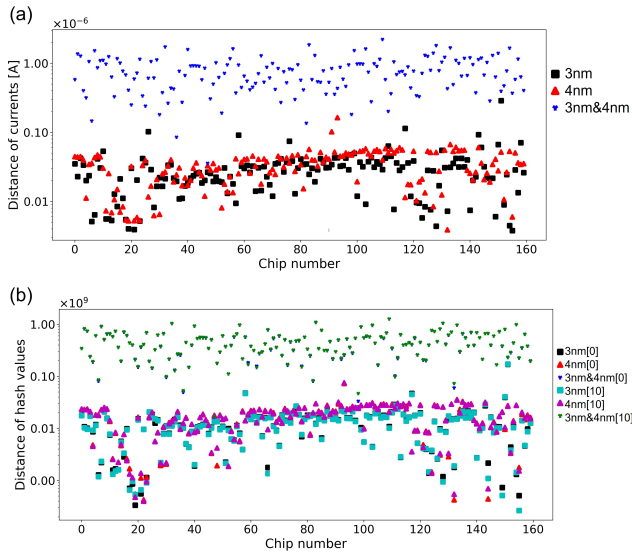


FIG. 3. (a) Euclidean distances between the datasets from day 1 and day 2 for 3 and 4 nm nanowire transistors. "3nm & 4nm" represents the Euclidean distance between the datasets of 3 nm-day1 and 4 nm-day1. (b) Differences in the hash values for the same dataset as in (a) for nanowire transistors. The random numbers $\{a, b\}$ are varied, where "[0]" and "[10]" correspond to the results from the first and 11 th sets of random numbers.

Fig. 5(b) has increased, making the distinction between the two devices more pronounced.

In summary, the application of LSH for device indexing was proposed to differentiate between nearly identical devices that are originally designed to exhibit the same characteristics. The LSH algorithm facilitates classification by generating simple hashed numbers, enabling an approximate but effective distinction between these devices. When multiple types of data, such as I_D - V_D and I_D - V_G , are available, combining their corresponding hashed identifiers improves classification accuracy. The determination of LSH parameters was demonstrated using experimental data from Coulomb blockade phenomena in PMOSFETs and nanowire transistors. This classification approach is expected to contribute to device performance enhancement by integrating feedback into the fabrication process.

DATA AVAILABILITY

The data that supports the findings of this study are available within the article.

ACKNOWLEDGMENTS

This work was supported by JSPS KAKENHI Grant Number JP22K03497.

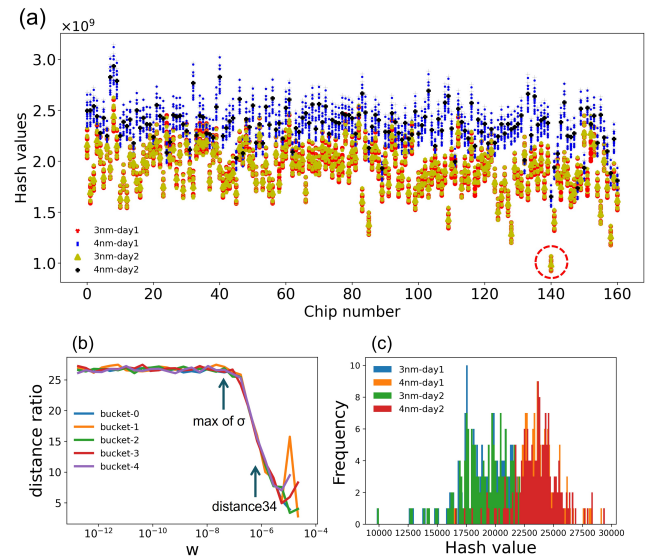


FIG. 4. (a) Hash values for the 3 and 4 nm nanowire transistors when the random numbers a and b are varied. The dotted circle highlights chip No. 141, corresponding to Fig. 2.(b)Histogram of hash value distributions. (c)Distance ratio defined Eq.(3) as the function of w .

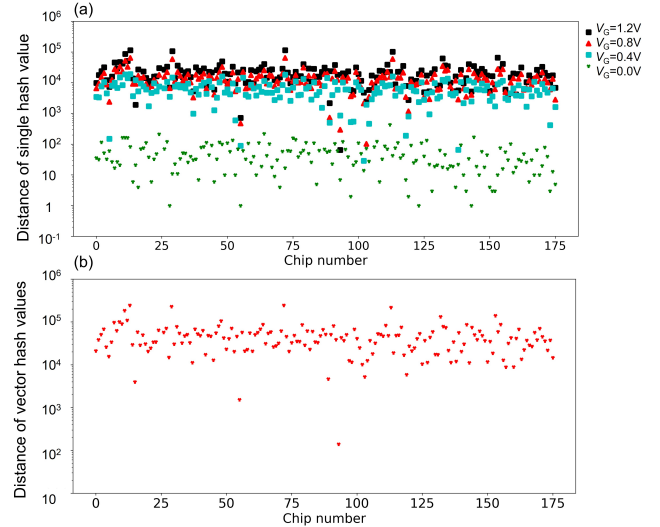


FIG. 5. (a) Distance of hash values of I_D - V_D of the 3 and 4 nm nanowires for different V_G s. (b) Distance of hash values of I_D - V_D of the 3 and 4 nm nanowires when the data (a) are treated as a vectors.

CONFLICT OF INTEREST

The authors have no conflicts to disclose.

Appendix A: clustering approach

We perform clustering analysis on silicon nanowire transistors using the Python scikit-learn library²⁰. Clustering algo-

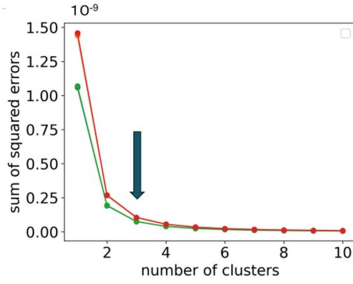


FIG. 6. Results of the elbow method to the I_D - V_D characteristics of the nanowire transistor. In the elbow method, the change of the "sum of the square error" represents the plausible number of the clusters.

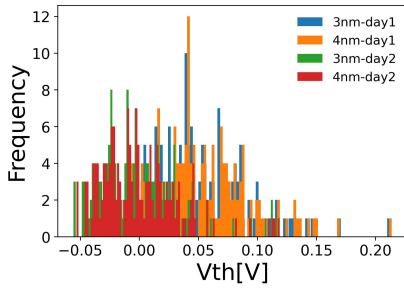


FIG. 7. Threshold voltage distributions for the 3nm and 4nm nanowire transistors.

gorithms help identify patterns in datasets, with K-means being one of the most widely used methods for partitioning data into k clusters. To determine an appropriate value for k , we apply the elbow method. Figure 6 presents the results of the elbow method, suggesting that the I_D - V_D data can be divided into approximately three clusters. This indicates that the dataset consists of similar transistor characteristics.

Next, we apply the k-means algorithm to partition the dataset. When selecting $k = 6$, the 168 transistors are categorized into distinct cluster numbers, as detailed in the following analysis. [4 5 2 3 4 2 4 1 3 4 5 2 5 4 1 2 2 1 1 4 4 3 4 2 3 4 4 2 4 2 3 1 2 4 3 4 3 2 4 4 1 2 2 2 1 5 4 4 3 4 1 2 3 2 1 2 5 4 2 4 4 3 1 4 1 1 2 4 4 1 1 4 4 4 1 4 1 1 3 1 4 4 3 5 4 0 4 4 1 2 1 2 3 4 2 2 4 5 3 5 2 2 1 2 1 1 2 2 1 0 1 1 3 2 1 2 4 2 1 4 1 1 4 2 5 5 2 5 0 1 2 2 4 2 1 1 2 4 2 1 0 0 1 2 1 1 5 1 2 3 2 3 4 2 5 1 2 0 2 5]. The clustering appears to progress sequentially from transistor No. 1 to No. 160. However, the distinct device (transistor No. 141 (underlined)) in Fig.2 (a)(b) is classified into the same cluster as transistors No. 142 and others. This instance indicates that the clustering was not entirely successful. Therefore, using k-means clustering to distinguish similar data may not always be effective.

Figure 7 displays the histogram of threshold voltages estimated using the conventional method. It is evident that the threshold voltages are randomly distributed among the four devices, making it impossible to distinguish between them.

Scale Integration of 2D Semiconductors for High-Performance Transistor Circuits", *Adv. Mater.* **34**, 2109796 (2022).

- ³J. Nam, S. Chun, G. Koo, Y. Kim, B. Moon, and J. Lim, "A New Wafer Level Latent Defect Screening Methodology for Highly Reliable DRAM Using a Response Surface Method", *IEEE International Test Conference*, Santa Clara, 1 (2008).
- ⁴M. Quach, Tuan Pham, T. Figal, B. Kopitzke and P. O'Neill, "Wafer-level defect-based testing using enhanced voltage stress and statistical test data evaluation", *International Test Conference*, Baltimore, 683 (2002).
- ⁵T. -H. Kim, W. Zhang, and C. H. Kim, "An SRAM reliability test macro for fully-automated statistical measurements of Vmin degradation", *IEEE Custom Integrated Circuits Conference*, San Jose, 231 (2009).
- ⁶N. Calik, F. Güneş, S. Koziel, A. Pietrenko-Dabrowska, M. A. Belen, and P. Mahouti, "Deep-learning-based precise characterization of microwave transistors using fully-automated regression surrogates", *Sci Rep* **13**, 1445 (2023).
- ⁷R. C. Y. Fang, R. D. Rung and K. M. Cham, "An improved automatic test system for VLSI parametric testing", *IEEE Transactions on Instrumentation and Measurement*, **IM-31**, 198 (1982).
- ⁸J. Guajardo, S. S. Kumar, G.-J. Schrijen, and P. Tuyls, "FPGA intrinsic PUFs and their use for IP protection", *9th Int. Workshop on Cryptographic Hardware and Embedded Systems*, Vienna, 63 (2007).
- ⁹D. E. Holcomb, W. P. Burleson, and K. Fu, "Power-up SRAM State as an Identifying Fingerprint and Source of True Random Numbers", *IEEE Trans. Comput.* **58**, 1198 (2009).
- ¹⁰T. Marukame, T. Tanamoto, and Y. Mitani, "Extracting Physically Unclonable Function From Spin Transfer Switching Characteristics in Magnetic Tunnel Junctions", *IEEE Trans. Mag.* **50**, 1 (2014).
- ¹¹G. E. Suh and S. Devadas, "Physical unclonable functions for device authentication and secret key generation", in *44th Ann. Design Automation Conf. San Diego*, 9 (2007).
- ¹²T. Tanamoto, S. Yasuda, S. Takaya, and S. Fujita, "Physically Unclonable Function using Initial Waveform of Ring Oscillators", *IEEE Trans. Circuits and Systems II: Express Briefs* **64**, 827 (2017).
- ¹³J. Chen, T. Tanamoto, H. Noguchi, and Y. Mitani, "Further investigations on traps stabilities in random telegraph signal noise and the application to a novel concept physical unclonable function (PUF) with robust reliabilities", *IEEE Symposium on VLSI Technology*, Kyoto, 40 (2015).
- ¹⁴T. Nagao, T. Nakamura, M. Kajiyama, M. Eiki, M. Inoue, and M. Shin-tani, "Wafer-Level Characteristic Variation Modeling Considering Systematic Discontinuous Effects", *28th Asia and South Pacific Design Automation Conference*, Tokyo, 442 (2023).
- ¹⁵T. Tanamoto, Y. Nishi, and K. Ono, "Application of single-electron effects to fingerprints of chips using image recognition algorithms", *Appl. Phys. Lett.* **115**, 033504 (2019).
- ¹⁶<https://opencv.org/>
- ¹⁷P. F. Alcantarilla, J. Nuevo, and A. Bartoli, "Fast explicit diffusion for accelerated features in nonlinear scale spaces", *British Machine Vision Conference*, Bristol (2013).
- ¹⁸S. Leutenegger, M. Chli, and R. Siegwart, "Brisk: Binary robust invariant scalable keypoints", *Int. Conf. Computer Vision* 2548 (2011).
- ¹⁹E. Rublee, V. Rabaud, K. Konolige, and G. Bradski, "ORB: An efficient alternative to SIFT or SURF", *IEEE International Conference on Computer Vision*, Barcelona, 2564 (2011).
- ²⁰<https://scikit-learn.org/1.5/modules/clustering.html>
- ²¹P. Indyk, and R. Motwani, "Approximate nearest neighbor:Towards removing the curse of dimensionality", *Symposium on Theory of Computing*, Dallas, 604 (1998).
- ²²A. Andoni and P. Indyk, "Near-Optimal Hashing Algorithms for Approximate Nearest Neighbor in High Dimensions", *47th Annual IEEE Symposium on Foundations of Computer Science*, Berkeley, 459 (2006).
- ²³M. Datar, N. Immorlica, P. Indyk, and V. S. Mirrokni, "Locality-sensitive hashing scheme based on p-stable distributions", the twentieth annual symposium on Computational geometry, Brooklyn, 253 (2004).
- ²⁴Y. Lu, X. Liu, A. Soltoggio, and S. Kolouri, "SLoSH: Set Locality Sensitive Hashing via Sliced-Wasserstein Embeddings", *IEEE/CVF Winter Conference on Applications of Computer Vision*, Waikoloa, 2554 (2024).
- ²⁵Y. Tian, X. Zhao, and X. Zhou, "DB-LSH 2.0: Locality-Sensitive Hashing With Query-Based Dynamic Bucketing", *IEEE Transactions on Knowledge and Data Engineering*, **36**, 1000 (2024).

¹S. K. Moore, "The node is nonsense," *IEEE Spectrum*, **57**, 24, (2020).

²T. Schram, S. Sutar, I. Radu, and I. Asselberghs, "Challenges of Wafer-

- ²⁶Y. Zhang, H. Lu, L. Zhang, X. Ruan, and S. Sakai, "Video anomaly detection based on locality sensitive hashing filters", *Pattern Recognition*, **59**, 302 (2016).
- ²⁷R. Cai, C. Zhang, L. Zhang, and W.-Y. Ma, "Scalable music recommendation by search", *15th ACM international conference on Multimedia, Augsburg*, 1065 (2007).
- ²⁸Y. Luo, Y. W. Yu, J. Zeng, B. Berger, and J. Peng, "Metagenomic binning through low-density hashing", *Bioinformatics*, **35**, 219 (2019).
- ²⁹B. Charyyev and M. Hadi Gunes, "Identifying Anomaly in IoT Traffic Flow With Locality Sensitive Hashes", *IEEE Access*, **12**, 89467 (2024).
- ³⁰K. Ono, T. Tanamoto, and T. Ohguro, "Pseudosymmetric bias and correct estimation of Coulomb/confinement energy for unintentional quantum dot in channel of metal-oxide-semiconductor field-effect transistor", *Appl. Phys. Lett.* **103**, 183107 (2013).
- ³¹K. Ono, G. Giavaras, T. Tanamoto, T. Ohguro, X. Hu, and F. Nori, "Hole Spin Resonance and Spin-Orbit Coupling in a Silicon Metal-Oxide-Semiconductor Field-Effect Transistor", *Phys. Rev. Lett.* **119**, 156802 (2017).
- ³²H. Qiu, K. Takeuchi, T. Mizutani, T. Saraya, J. Chen, M. Kobayashi "Statistical Analyses of Random Telegraph Noise Amplitude in Ultra-Narrow (Deep Sub-10nm) Silicon Nanowire Transistors", *IEEE Symposium on VLSI Technology, Kyoto*, 50 (2017).
- ³³T. Mizutani, Y. Tanahashi, R. Suzuki, T. Saraya, M. Kobayashi, and T. Hiramoto, "Threshold voltage and current variability of extremely narrow silicon nanowire MOSFETs with width down to 2nm", *IEEE Silicon Nanoelectronics Workshop, Kyoto*, 1 (2015).
- ³⁴T. Mizutani, K. Takeuchi, R. Suzuki, T. Saraya, M. Kobayashi, and T. Hiramoto, "Increased drain-induced variability and within-device variability in extremely narrow silicon nanowire MOSFETs with width down to 2nm", *IEEE Silicon Nanoelectronics Workshop, Honolulu*, 138, (2016).
- ³⁵R. Suzuki, M. Nozue, T. Saraya and T. Hiramoto, "Experimental Observation of Quantum Confinement Effect in <110> and <100> Silicon Nanowire Field-Effect Transistors and Single-Electron/Hole Transistors Operating at Room Temperature", *Jpn. J. Appl. Phys.* **52**, 104001 (2013).